Energy efficiency of pulse shaping in electrical stimulation: the interdependence of biophysical effects and circuit design losses

Varkevisser, F.; Lopes Marta da Costa, T.M.; Serdijn, W.A.
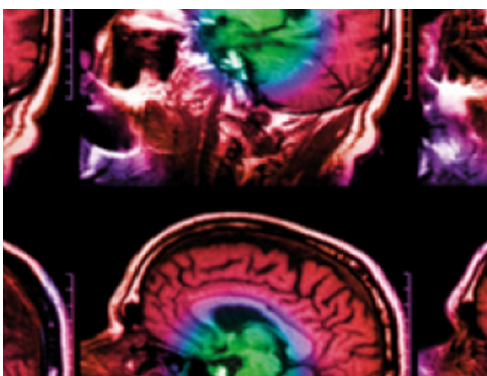
PAPER • OPEN ACCESS

Energy efficiency of pulse shaping in electrical stimulation: the interdependence of biophysical effects and circuit design losses

To cite this article: Francesc Varkevisser *et al* 2022 *Biomed. Phys. Eng. Express* **8** 065009

View the article online for updates and enhancements.

Biomedical Physics & Engineering Express

PAPER

Energy efficiency of pulse shaping in electrical stimulation: the interdependence of biophysical effects and circuit design losses

Francesc Varkevisser , Tiago L Costa and Wouter A Serdijn

Section Bioelectronics, Department of Microelectronics, Delft University of Technology, 2628CD Delft, The Netherlands

E-mail: f.varkevisser@tudelft.nl

Abstract

Power efficiency in electrical stimulator circuits is crucial for developing large-scale multichannel applications like bidirectional brain-computer interfaces and neuroprosthetic devices. Many state-of-the-art papers have suggested that some non-rectangular pulse shapes are more energy-efficient for exciting neural excitation than the conventional rectangular shape. However, additional losses in the stimulator circuit, which arise from employing such pulses, were not considered. In this work, we analyze the total energy efficiency of a stimulation system featuring non-rectangular stimuli, taking into account the losses in the stimulator circuit. To this end, activation current thresholds for different pulse shapes and durations in cortical neurons are modeled, and the energy required to generate the pulses from a constant voltage supply is calculated. The proposed calculation reveals an energy increase of 14%–51% for non-rectangular pulses compared to the conventional rectangular stimuli, instead of the decrease claimed in previous literature. This result indicates that a rectangular stimulation pulse is more power-efficient than the tested alternative shapes in large-scale multichannel electrical stimulation systems.

1. Introduction

Electrical brain stimulation devices are successfully applied to treat several neural disorders such as Parkinson's disease, hearing loss, and visual impairment. Applications like bidirectional brain-computer interfaces and cortical visual stimulation drive the development of large-scale multichannel stimulator systems. These fully implantable devices interface with the brain by means of electrical pulses through hundreds to thousands of stimulation channels [1]. If battery operation is not an option, the power is transferred to the system via a wireless link. Due to safety regulations, the maximum deliverable power is limited. Therefore, the power efficiency of the stimulator needs to be optimized to increase the number of channels that can be stimulated with the available power.

Current Mode Stimulation (CMS) is often favored over Voltage Mode Stimulation (VMS) due to its inherent control over the injected charge, which is essential for safe operation [2]. However, conventional CMS is power inefficient, especially in multichannel

devices [3]. A generic circuit diagram for CMS is depicted in figure 1(a). Rectangular current pulses are generated from a fixed voltage supply and applied to the tissue impedance, Z_{tis}. Switches SW_1 and SW_2 are used to change the direction of the current through Z_{tis}, such that a bipolar pulse is applied to the tissue. The voltage supply needs to be sufficiently high to cope with the voltage drop across the tissue and the overhead voltage required for the current source. The amplitude of V_{load} depends on the amplitude of the current pulse and Z_{tis}, which can be highly variable for different channels in the same system. Any mismatch between V_{supply} and V_{load} leads to a voltage drop across the source I_{stim}, indicated by the grey area in figure 1(b), resulting in energy dissipation —and thus inefficiency—in the current source. In a multichannel system, the voltage supply needs to accommodate the worst-case channel. Therefore, all other channels operate at an unnecessarily high supply voltage, which results in energy waste.

One method to reduce energy consumption in CMS is pulse shaping. Several studies suggest that non-rectangular stimulation pulses might be more energy-efficient

Figure 1. (a) Generic circuit diagram for current mode stimulation in a bipolar electrode configuration. (b) Example of rectangular pulses generated by I_{stim} consisting of two phases with equal amplitudes and durations, separated by an interphase delay. During the interphase delay, SW_1 and SW_2 will switch to direct the current through the tissue in the opposite direction during the second phase. (c) Resulting voltage at node V_{load} for a typical tissue load, and the fixed supply voltage. The shaded grey area indicates the voltage drop across I_{stim} as a result of a mismatch between V_{supply} and V_{load}.

than the conventional rectangular stimulation pulses [4–7]. Computational studies using detailed neuron models evaluated the efficiency of alternative shapes. The energy consumption of different pulse shapes for deep brain stimulation was modeled in [4]. Centered-triangular and Gaussian-shaped pulses reduced the energy consumption by approximately 10% compared to the energy-optimal rectangular pulse. In [5], a genetic algorithm was developed to find a pulse shape optimized for energy efficiency. The resulting pulse resembled a truncated Gaussian curve. When comparing the optimized pulses to rectangular pulses of equal duration in the range of 50–200 μs, a decrease in activation energy ranging from 5% to 60% was observed. However, compared to the energy-optimal rectangular pulse, the maximum energy-saving was approximately 20%. The efficiency of Gaussian-shaped pulses was investigated *in vivo* in [6]. A decrease in activation energy of 17% was reported in the pulse width range of 50-200 μs. Research consistently reports that non-rectangular pulses (preferably Gaussian or centered-triangular) can be more energy-efficient, but it is acknowledged that possible circuit implications could alter this conclusion [5]. What is mostly overlooked in the literature, is that non-rectangular pulses alter the required compliance voltage required at stimulation output stages due to an increase in the peak current. This will cause an increase in the overhead energy losses in the output stage of the device.

A possible solution to reduce the overhead losses in CMS is dynamic voltage scaling (DVS) [8–15]. In DVS, the supply voltage is dynamically scaled to minimize the voltage drop across the current driver. Generally, state-of-the-art DVS techniques can be divided into two methods. The first method scales the supply voltage by modulating the incoming AC power signal [8, 9]. The second method uses (on-chip) adaptive DC/DC converters, for example, inductive buck/boost converters [10, 11] or switched-capacitor charge pumps [12–15]. The signal modulation and inductive DC/DC converter approaches benefit from a continuous output voltage range but suffer from limited

scalability. Inductor-based converters require bulky off-chip inductor(s) for each channel, and modulation of the incoming power signal only allows for the adaptation of a single channel. Alternatively, switched-capacitor-based converters allow for a fully integrated implementation that can be shared by many channels but have limited output resolution. This method produces discrete voltage steps, and each step occupies a relatively large area. Therefore, they are usually limited to only a few voltage steps.

Foutz *et al* [16] suggested that non-rectangular pulse shapes should be combined with scaling of the (constant) voltage supply for optimal energy efficiency. However, they analyzed both methods separately and did not consider the effect of the non-rectangular shapes on the required voltage compliance. It is important to note that the two methods described above reduce the energy consumption of electrical stimulation in two different domains. Voltage scaling techniques reduce overhead energy consumption in the electrical domain, whereas pulse shaping techniques reduce the activation energy in the biological domain. To the best of the authors' knowledge, an efficiency analysis considering both methods concurrently is yet to be performed.
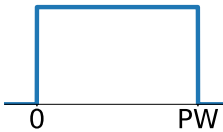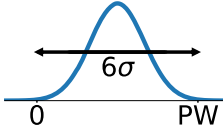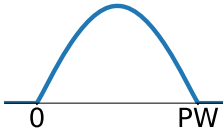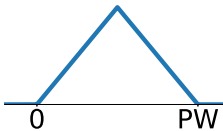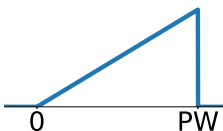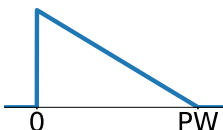
This work presents a high-level analysis of the total energy efficiency of pulse shaping techniques generated from scaled voltage supplies. We do so by analyzing the activation thresholds of different pulse configurations on computational models of cortical neurons—both for biophysically realistic neuron models [17] and for a straight axon model.

2. Methods

2.1. Stimulation waveforms
We analyzed the current thresholds for monophasic, cathodic stimulation pulses of different shapes. The used shapes are: rectangular, Gaussian, half-sine, centered triangular, ramp-up, and ramp-down. The

Table 1. Illustration of the used pulse shapes.

Name	Shape
Rectangular	
Gaussian	
Half-Sine	
Triangular	
Ramp-Up	
Ramp-Down	

definitions of the pulse shapes are listed in appendix A and illustrated in table 1. For the Gaussian-shaped pulses, the pulse width (PW) was defined as 6σ. All other shapes were non-zero for $0 \leqslant t \leqslant$ PW and zero otherwise.

2.2. Neuron models

We used two types of neuron models in the NEURON v8.0 simulation software [18]: a single-axon fiber model and the biophysically realistic models presented in [17]. We will focus on the results for the single-axon fiber for most of this work to ease the interpretation of the results. For both models, extracellular electrical stimulation was modeled in a homogeneous, isotropic environment. A point-source electrode delivered the pulses. The spatial component of the electric field along the membrane was calculated using (1), where σ

is the extracellular conductivity and r is the distance to the electrode.

$$V_e(r) = \frac{1}{4\pi\sigma r} \tag{1}$$

The calculated extracellular potential was applied to each section of the model using NEURON's 'extracellular' mechanism. In each time step, the potential was scaled proportionally to the current amplitude of the stimulus.

2.2.1. Axon fiber model

The single-axon fiber model is a multi-compartment single-cable model that consists of 101 active nodal sections, representing nodes of Ranvier, connected by 100 passive inter-nodal sections, representing myelin sheath. The fiber dimensions and membrane dynamics are based on the axonal b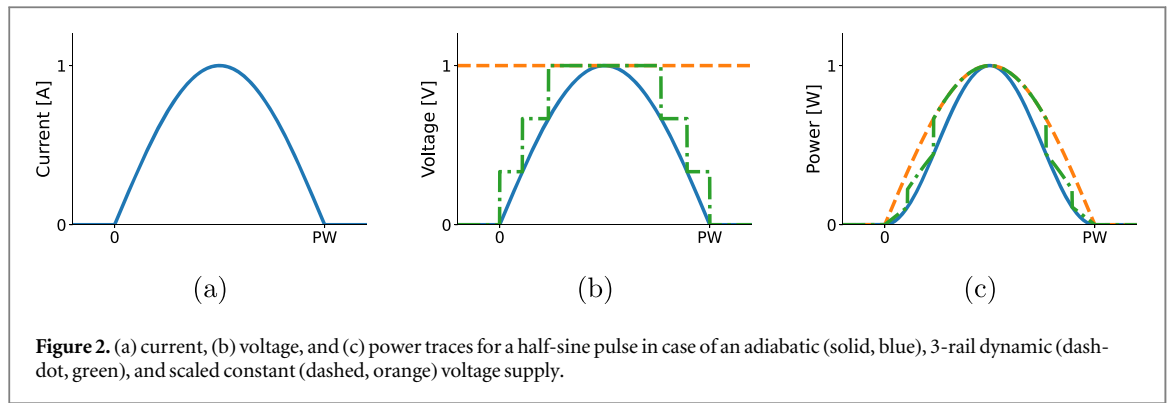ranch of a human L5 thick-tufted pyramidal cell [17]. The inter-nodal sections only have passive membrane properties, while the nodal sections have both passive and active properties. The active properties of the nodal sections include five Hodgkin-Huxley-like ion channels: transient sodium, persistent sodium, transient potassium, persistent potassium, and A-type potassium (Kv3.1) [17]. The model properties are listed in table B1 appendix B.

The electrode was positioned directly above the center node at a distance of 100 μm. Simulations were run with a time step of 0.1 μs using implicit Euler integration. A stimulus was considered supra-threshold if the outermost nodes' membrane voltage (V_m) crossed 0 mV. Activation thresholds were determined to an accuracy of 10^{-2} μA using a binary search algorithm for PWs ranging from 10 μs to 1 ms in steps of 10 μs.

2.2.2. Biophyisically realistic models

In [17], 25 biophysically realistic neuron models representing neurons in different cortical layers are presented. In this work, we used the five L5 cells as an extra validation step to account for the effects of cell-electrode distance and cell morphology on shape dependency.

The electrode was placed in a grid of equally spaced locations around the cells, separated by steps of 200 μm in x, y, and z directions. The boundaries of the grid were determined by the extremities of the cell geometry in all three directions. All locations with a distance to any part of the cell smaller than 30 μm or larger than 500 μm were removed from the locations set. This resulted in a set of 1800 locations divided over the five models. The time step for these simulations was 5 μs. A stimulus was considered supra-threshold if the membrane voltage at the soma crossed 0 mV. Current thresholds were determined for PWs ranging from 10 μs to 1.5 ms in steps of 50 μs to an inaccuracy of <1%. Locations where the optimal energy point for any of the shapes was at maximum pulse duration were omitted, as this might indicate that the minimum energy point has not been reached yet. Consequently, a total of 1561 locations are included in the results.

Figure 2. (a) current, (b) voltage, and (c) power traces for a half-sine pulse in case of an adiabatic (solid, blue), 3-rail dynamic (dash-dot, green), and scaled constant (dashed, orange) voltage supply.

2.3. Shape comparisons

After determining the thresholds for all pulse configurations, we compared the pulse shapes on different metrics. First, the shapes are compared by the peak current at threshold conditions for different PWs in a Strength-Duration curve. Next, the charge threshold of each shape is calculated using (2), and Charge-Duration curves are used to compare the shapes.

$$Q_{\text{th}} = \int_0^{PW} I(t)\,\mathrm{d}t \qquad (2)$$

Furthermore, the energy of each shape is calculated for two scenarios. First, the energy is calculated using (3), which corresponds to energy calculations of stimulation pulses reported in previous literature [4, 5].

$$E_{\text{adiabatic}} = \int_0^{PW} P(t)\,\mathrm{d}t$$
$$= \int_0^{PW} V(t)I(t)\,\mathrm{d}t \propto \int_0^{PW} I(t)^2\,\mathrm{d}t \qquad (3)$$

In (3), the quasi-static approximation [19] is used to scale the voltage proportionally to the current. As the voltage is proportional to the current, this would require a fully adaptive (adiabatic) voltage supply for the non-rectangular pulses in a practical system.

Second, we consider the case where the current is generated from a constant voltage supply. In this calculation, we scaled the voltage proportional to the peak current of the pulse. This scenario combines pulse shaping and voltage scaling, as proposed in [16]. The energy required to generate the pulse in this case is calculated using:

$$E_{\text{constant}} = V_{\text{constant}} \int_0^{PW} I(t)\,\mathrm{d}t \propto I_{\text{peak}}$$
$$\times \int_0^{PW} I(t)\,\mathrm{d}t = I_{\text{peak}} \cdot Q \qquad (4)$$

To illustrate the difference between the calculations, the current, voltage, and power traces in the case of an adiabatic and scaled constant supply voltages are compared in figure 2 for the example of a half-sine pulse.

For both energy calculations, we calculate the relative energy efficiency of the shapes using (5), where E_x is the threshold energy for shape x, and E_r is the energy needed for a rectangular pulse. Thus, a negative number indicates a decrease in energy with respect to the rectangular pulse, while a positive number indicates an increase in energy. The energy efficiency is assessed based on the minimum required energy for each shape rather than for each PW because the PW definition for non-rectangular pulses can be chosen freely. Consequently, a PW-bound comparison would depend on the chosen definition [16].

$$\eta_{\text{E}} = \left(\frac{\min(E_x)}{\min(E_r)} - 1 \right) \cdot 100\% \qquad (5)$$

In calculating the energy efficiency for the case of a constant supply, it is assumed that the voltage is scaled proportionally to I_{peak} to maximize efficiency. However, in a practical system, the voltage is usually fixed and can not be scaled to its optimal value at each channel. It shows from (4) that if V_{supply} is fixed, only a decrease in Q can lower the energy threshold. Therefore, we compare the shapes by their Strength-Charge (I_{th} versus Q) relationship to evaluate energy efficiencies for a fixed supply.

2.4. Dynamic voltage scaling

As demonstrated in [20], dynamic voltage scaling could improve the energy efficiency for non-rectangular pulses. The total efficiency, including dynamic voltage scaling, can be calculated using:

$$\eta_{\text{total,dvs}} = \eta_{\text{const}} \cdot \eta_{\text{dvs}}, \qquad (6)$$

where η_{const} is the efficiency of generating the pulses from a constant supply as presented in this work, and η_{dvs} is the potential efficiency of applying the dynamic voltage scaling technique as shown in [20]. η_{dvs} is calculated using (7), where E_{dvs} is the required energy in the case of dynamic voltage scaling. In that case, the supply voltage consists of a number of distinct voltage rails and is stepped towards the lowest possible voltage to accommodate the stimulation current at each point in time. In figure 2, dynamic voltage scaling is illustrated for the example of a 3-rail supply.

$$\eta_{\text{dvs}} = \left(\frac{E_{\text{constant}}}{E_{\text{dvs}}} - 1 \right) \cdot 100\% \qquad (7)$$

2.5. Capacitive effects of electrode-tissue interface

In the previous sections, Z_{tis} is assumed to be resistive in all calculations. A more realistic model includes

Figure 3. Current threshold for different pulse shapes and widths in the single-axon fiber model. The reported threshold is the peak current of the pulses, and the pulse widths are defined in appendix A.
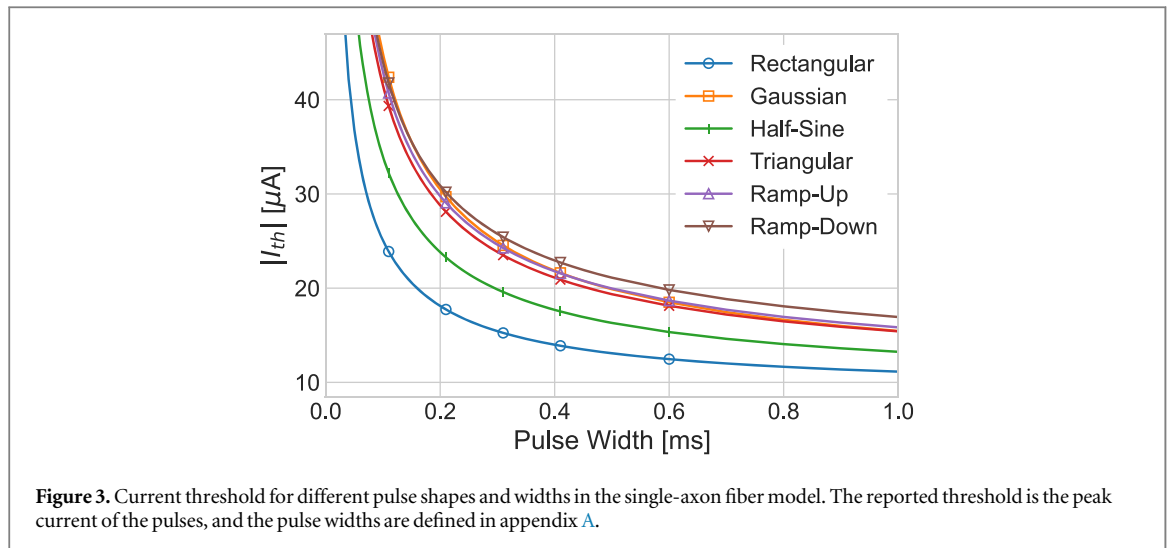
the electrode-tissue interface (ETI), which has a capacitive nature. Including the ETI will result in reactive components in the voltage during current-controlled stimulation pulses. The amplitude of this effect depends on the geometry and material of the electrodes. Generally, electrodes for electrical stimulation should be designed to minimize the voltage drop over the ETI to prevent harmful electrochemical reactions [21]. For this reason, the error introduced by the assumption of a resistive load should be small. Nevertheless, for completeness of our analysis, we consider the capacitive effects of the ETI in this section.

To include ETI effects, the load of a stimulator circuit is commonly modeled as a combination of a tissue resistance (R_s) in series with a double layer capacitance (C_{dl}). During a current pulse, C_{dl} will be charged, causing an increase in the load voltage. To account for the capacitive charging, the load voltage can be calculated using (8), where $\tau = R_s C_{dl}$.

$$V_{load}(t) = R_s \cdot I(t) + \frac{1}{C_{dl}} \int_0^t I(t)\,dt$$
$$= R_s\left(I(t) + \frac{1}{\tau} \int_0^t I(t)\,dt\right) \qquad (8)$$

The peak voltage of shape x will increase by a factor β_x as described by (9).

$$\beta_x = \frac{\max[V_{load}(t)|_{1/\tau > 0}]}{\max[V_{load}(t)|_{1/\tau = 0}]} \qquad (9)$$

Consequently, the energy calculation for the constant-supply-voltage scenario can be expanded to (10) to account for C_{dl}.

$$E_{rc,x} = \beta_x \cdot E_{constant,x} = \beta_x \cdot I_{peak} \cdot Q \qquad (10)$$

To compare the effect of C_{dl} between rectangular and non-rectangular shapes, we use (11).

$$\eta_\beta = \left(\frac{\beta_x}{\beta_r} - 1\right) \cdot 100\% \qquad (11)$$

3. Results

3.1. Single-axon fiber model

The strength-duration behavior of all shapes was monotonically decreasing (figure 3). For short PWs, all strength-duration curves approach a vertical asymptote, while for long PWs, they approach a horizontal asymptote. For all PWs, rectangular pulses had the lowest threshold and ramp-down pulses the highest.

Furthermore, all shapes had monotonically increasing charge thresholds with increasing PW (figure 4). For all PWs, rectangular pulses had the highest charge threshold, and Gaussian pulses the lowest.

In the case of an adiabatic voltage supply, the energy-duration curves show potential energy savings for non-rectangular pulses (figure 5(a)). For PWs >150 μs, the rectangular pulses were the least energy-efficient. The energy-optimal shape is PW dependent, but the lowest energy can be achieved using Gaussian pulses with a PW of 240 μs. The energy efficiencies for the non-rectangular pulses in the case of an adiabatic voltage supply are listed in table 2.

The energy-duration relationships change when the pulses are generated from a scaled constant voltage supply (figure 5(b)). Still, no single shape is the most energy-efficient for all PWs; however, the overall least energy can now be achieved with rectangular pulses with a duration of 110 μs. For PWs <440 μs, rectangular pulses have the lowest energy threshold. For longer PWs, the Gaussian pulses require the least amount of energy. The energy efficiencies of non-rectangular pulses in the case of a constant voltage supply are listed in table 3.

To compare the efficiency in the case of a fixed voltage supply, the current-charge relationship for the different pulse shapes is depicted in figure 6. As explained in section 2.3, only a decrease in charge can lower the energy when the supply voltage is fixed. Therefore, a lower charge threshold for a given I_{th} (proportional to V_{supply}) means better energy performance of a circuit generating that pulse from a constant voltage.
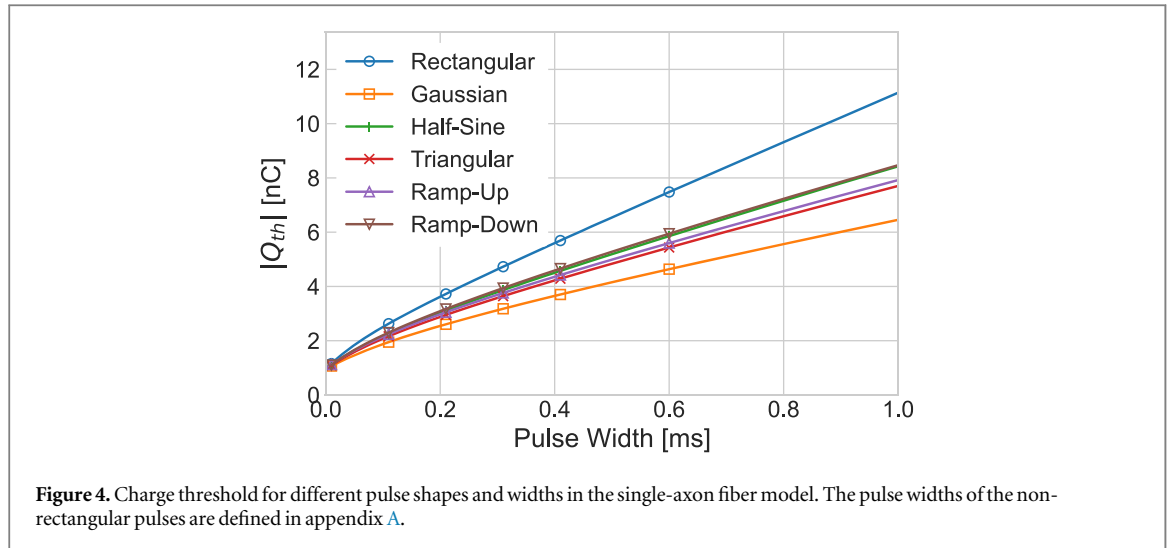
Figure 4. Charge threshold for different pulse shapes and widths in the single-axon fiber model. The pulse widths of the non-rectangular pulses are defined in appendix A.
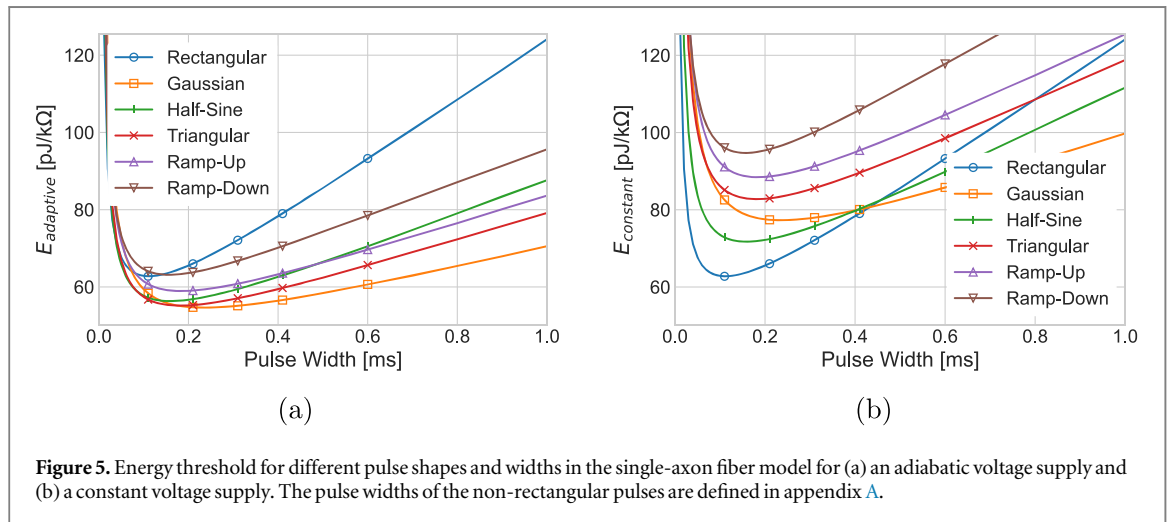

Figure 5. Energy threshold for different pulse shapes and widths in the single-axon fiber model for (a) an adiabatic voltage supply and (b) a constant voltage supply. The pulse widths of the non-rectangular pulses are defined in appendix A.

Table 2. Relative energy efficiency of non-rectangular pulses with respect to rectangular pulses in the single-axon fiber model for an adiabatic voltage supply.

	Rectangular	Gaussian	Half-Sine	Triangular	Ramp-Up	Ramp-Dow
min(E) [pJ/kΩ]	62.8	54.6	56.3	55.2	58.9	63.1
η_E [%]	—	−12.9	−10.2	−12.1	−6.1	+0.6

Table 3. Relative energy efficiency of non-rectangular pulses with respect to rectangular pulses in the single-axon fiber model for a constant voltage supply.

	Rectangular	Gaussian	Half-Sine	Triangular	Ramp-Up	Ramp-Down
min(E) [pJ/kΩ]	62.8	77.3	71.7	82.8	88.4	94.7
η_E [%]	—	+23.2	+14.3	+31.9	+40.6	+50.9

Rectangular pulses have the lowest charge threshold for all values of I_{th}, while ramp-down pulses have the highest charge threshold for all values of I_{th}.

3.2. Biophysically realistic models

The energy efficiencies for adiabatic and constant-voltage supplies in the biophysically realistic models are shown in figure 7. The results show similar trends as the single-axon fiber model, supporting the validity of that model. In the case of an adiabatic voltage supply, non-rectangular pulses are more efficient, except for the ramp-down pulses. However, when considering the cost of generating the pulses from a constant supply, an energy increase ranging from 15.9 ± 1.1% (mean ± std %) for half-sine pulses to 51.7 ± 2.5% for triangular pulses is observed.
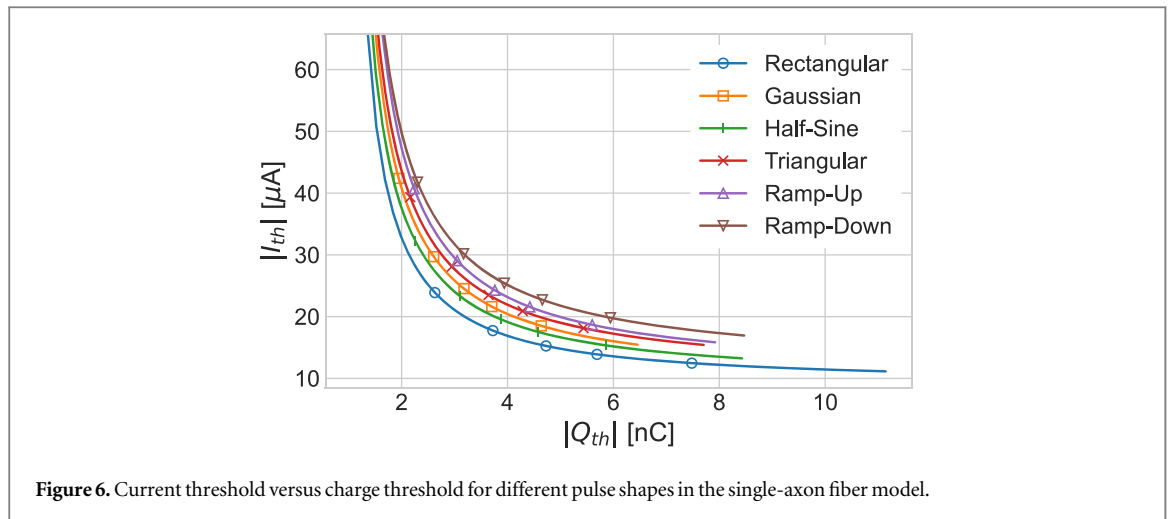
Figure 6. Current threshold versus charge threshold for different pulse shapes in the single-axon fiber model.
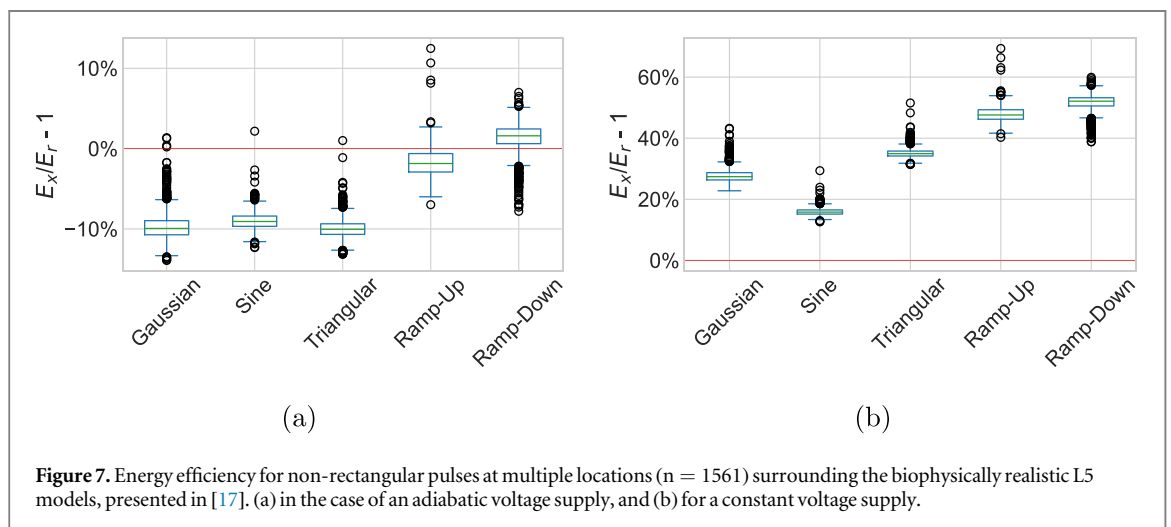

Figure 7. Energy efficiency for non-rectangular pulses at multiple locations (n = 1561) surrounding the biophysically realistic L5 models, presented in [17]. (a) in the case of an adiabatic voltage supply, and (b) for a constant voltage supply.

3.3. Dynamic voltage scaling

Potential energy savings for non-rectangular pulses by scaling the supply voltage to the instant requirements of the channel were calculated in [20]. For a multi-level DC/DC converter with six output steps, this results in an energy reduction of −22%, −15%, and −26% for Gaussian, half-sine, and triangular pulses, respectively. The total efficiency, calculated using (6), for different numbers of voltage steps is listed in table 4. The table shows an increase in energy for most of the shapes. Only in the case of a supply with more than four rails for the Gaussian and half-sine pulses or more than five rails for triangular pulses do they become slightly more efficient than rectangular pulses.

3.4. Effect of capacitive ETI

Large-scale multichannel devices will typically interface with arrays of microelectrodes. For microelectrodes, the order of magnitude for the model parameters are $R_s \approx 100\,k\Omega$ [22–24] and $C_{dl} \approx 10$–100 nF [25, 26]. Thus, the expected range of τ is 1–10 ms. Figure 8 depicts η_β for different values of τ over the relevant PW range. The effect of capacitive charging is highly dependent on τ and PW. The energy-duration

curves depicted in figure 9 account for different values of τ, and the total energy efficiencies are listed in table 5. In the expected range of τ, the rectangular pulse is still the most energy-efficient shape. However, its efficiency is affected, especially for longer pulse widths. Next to that, lower values of τ affect the rectangular pulses even further, and at $\tau = 0.1$ ms, the rectangular pulses are not optimal anymore. However, in the development of electrodes for stimulation, the capacitive transfer should be minimized [27] which will result in high values of τ. Therefore, the capacitive effect is expected to be reduced with further improvement of microelectrodes.

3.5. Generalization of results

Using the mathematical descriptions of the pulse shapes, one could generalize the obtained results of the proposed energy calculation to other scenarios (e.g., other models or experimental results). By combining equations (2) and (4), one can calculate the relative threshold value for which the required energy of an arbitrary shape becomes less than that of a rectangular pulse. As an example, the ratio of current thresholds that lead to equal required energy for the triangular

Table 4. Overall relative energy efficiency in % of non-rectangular stimulation pulses with respect to rectangular pulses for a system employing dynamic voltage scaling with various numbers of supply rails.

	$\eta_{\text{total,dvs}}$				
# Supply rails	Gaussian	Half-sine	Triangular	Ramp-up	Ramp-down
1	23.2	14.3	31.9	40.9	50.9
2	8.5	6.7	15.5	23.2	32.3
3	2.5	2.5	7.5	14.7	23.3
4	−0.9	0.0	3.1	10.0	18.2
5	−3.0	−1.7	0.3	7.0	15.0
6	−4.4	−2.9	−1.6	4.9	12.8

and rectangular pulses is given in (12*a*)–(12*c*).

$$E_{\text{const,r}} = I_{\text{th,r}} \cdot Q_{\text{th,r}} = I_{\text{th,r}}^2 \cdot PW \tag{12A}$$

$$E_{\text{const,t}} = I_{\text{th,t}} \cdot Q_{\text{th,t}} = I_{\text{th,t}}^2 \cdot \frac{PW}{2} \tag{12B}$$

$$E_{\text{const,r}} = E_{\text{const,t}} \Rightarrow \frac{I_{\text{th,t}}}{I_{\text{th,r}}} = \sqrt{2}. \tag{12C}$$

The threshold ratios are calculated similarly for the other shapes used in this work and summarized in table 6. The reported ratios are calculated for the shape definitions of this work. To use this method to compare the results of other works, one should recalculate the threshold ratio for the appropriate shape definitions. Furthermore, one could combine the ratio with η_{dvs} and/or η_β to include the effects of dynamic voltage scaling and capacitive charging, respectively.

4. Discussion

This study aimed to provide an energy efficiency analysis of different pulse shapes in electrical stimulation that includes losses in the generator circuit. Previously, it was suggested that the combination of non-rectangular pulses and an adjustable compliance voltage would result in the most energy-efficient way of stimulation [16]. First, we presented shape-dependent threshold characteristics for two types of neuron models. In line with previous literature, non-rectangular pulses decreased the charge threshold, while an increase in the strength-duration (current threshold) was observed. When the activation energy is calculated using (3) (assuming an adiabatic voltage supply), non-rectangular pulses show better energy efficiency. However, implementing an adiabatic voltage supply is costly in both area and power. Therefore, large-scale multichannel stimulator systems will typically have limited flexibility in the voltage supply. To account for the losses in the stimulator circuit due to this limited flexibility, we proposed an alternative energy calculation in (4). The results show that the efficiency of non-rectangular pulses is degraded in the proposed energy calculation. This is mainly due to an increase in the peak current, requiring a higher voltage supply.

The losses in the stimulator circuit can partially be reduced using dynamic voltage scaling. We have shown the potential energy reduction in the case of non-rectangular pulses for voltage supplies with up to 6 supply rails. However, it should be noted that the presented efficiencies can only be achieved for channels requiring full-range voltage output. Channels with lower impedance or amplitude requirements can not use all voltage steps, resulting in a decreased efficiency compared to rectangular pulses. As a result, most channels will operate at voltages below the full range in large-scale multichannel systems. Consequently, using rectangular pulses will result in the lowest overall energy consumption of the complete system. Nevertheless, multichannel stimulators can still benefit from voltage scaling when using rectangular pulses. Dynamic voltage scaling saves most energy for channels requiring sub-full-range amplitudes [20]. This is also true for rectangular pulses; thus, the total power consumption of a multichannel stimulator can be reduced by deploying independent voltage supply rails.

The pulse shapes used in this work are not always identical to the ones used in previous works, which might have an effect on the obtained results. The Gaussian-like pulses in [5] were truncated at the tails for small pulse widths, while [6] used Gaussian pulses with a fixed σ for all pulse widths. Furthermore, this work focused on monophasic pulses, while biphasic pulses are commonly used in electrical stimulation applications. The second phase—also called the recovery phase—is introduced to recover the charges applied during the first phase to prevent harmful electrochemical reactions [21]. The biphasic pulses can be symmetrical (the shape, amplitude, and duration of the second phase are equal to the first phase) or asymmetrical, but the total charge of both phases should be equal for safety. Previous work has shown that the introduction of the recovery causes an increase in the stimulation threshold compared to monophasic pulses [28]. However, many factors change the extent of this effect. For example, introducing an interphase delay and using asymmetrical pulses reduce the threshold increase [21, 29]. We used monophasic pulses to focus on the effects of pulse shaping of the first
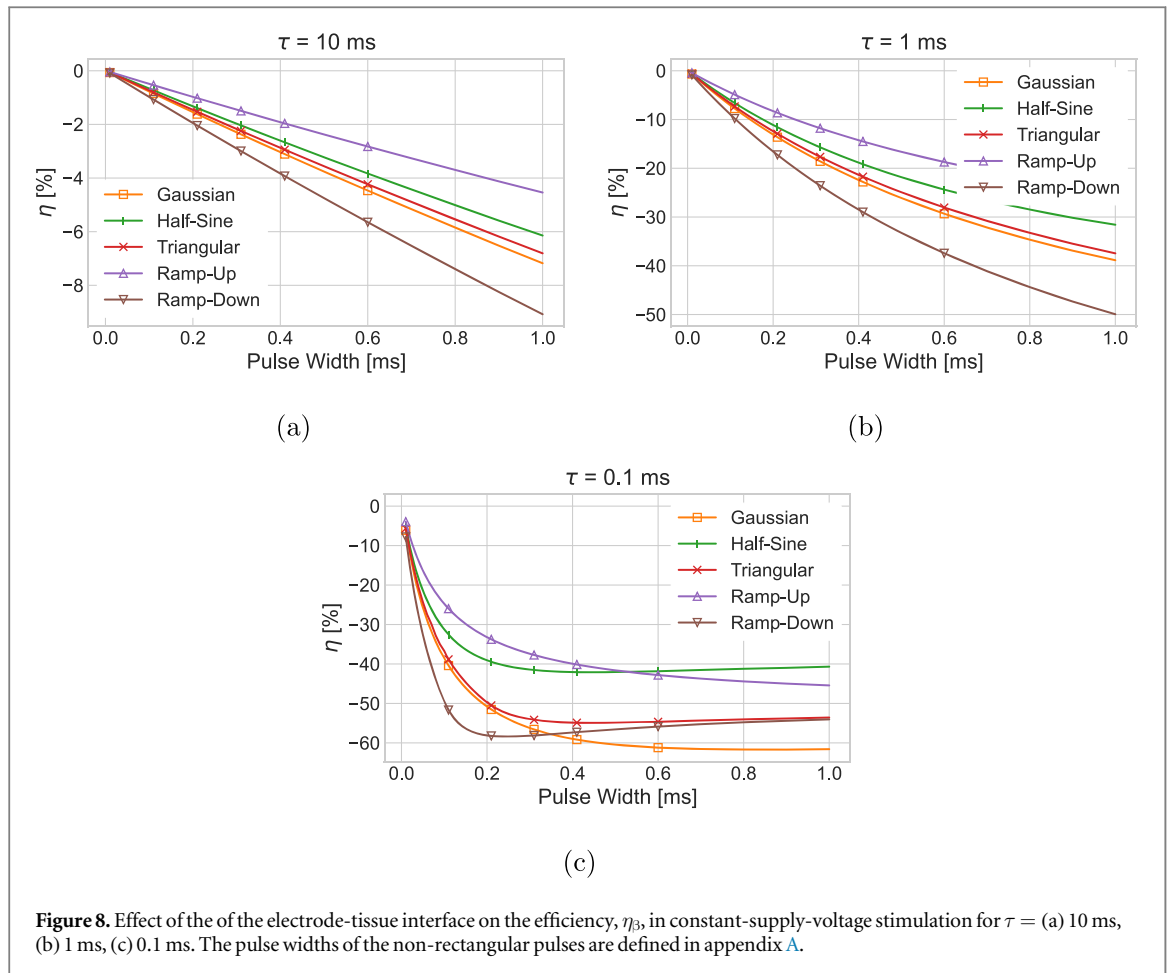
Figure 8. Effect of the of the electrode-tissue interface on the efficiency, η_β, in constant-supply-voltage stimulation for $\tau =$ (a) 10 ms, (b) 1 ms, (c) 0.1 ms. The pulse widths of the non-rectangular pulses are defined in appendix A.

Table 5. Overall relative energy efficiency in % of non-rectangular stimulation pulses with respect to rectangular pulses, taking into account charging of the double layer capacitance C_{dl}.

	$\eta_{total,\beta}$				
τ [ms]	Gaussian	Half-sine	Triangular	Ramp-up	Ramp-down
∞	23.2	14.3	31.9	40.9	50.9
10	22.4	13.6	31.0	40.6	49.3
1	17.7	9.4	25.7	39.0	38.1
0.1	3.9	-2.26	8.7	33.8	-1.85

phase without additional factors of the second phase. Since the second phase is not used to activate the cell, its shape and duration can be designed to minimize the energy consumption, regardless of the shape of the first phase.

The presented analysis does not include any losses introduced by additional circuitry required to generate non-rectangular pulses. The generation of rectangular pulses is relatively easy using a constant current source, while the generation of non-rectangular pulses requires additional circuitry [30, 31]. The power consumption of the additional circuits depends on the specific implementation and can be optimized, but it will degrade the efficiency of non-rectangular pulses even further.

Finally, the results presented in this work are based on the quasi-static approximation in a homogeneous and isotropic environment. This model exhibits various limitations due to the simplifications made. For example, it does not consider capacitive wave propagation through the tissue. Thus, it is unlikely that the exact percentages presented here will translate to an in-vivo environment. Further research is required to incorporate these effects into the energy calculations.

5. Conclusion

Non-rectangular pulses are often presented to be more energy-efficient than rectangular pulses for electrical stimulation. We have shown that it is crucial to incorporate the cost of generating such pulses in assessing energy efficiency. The presented results suggest
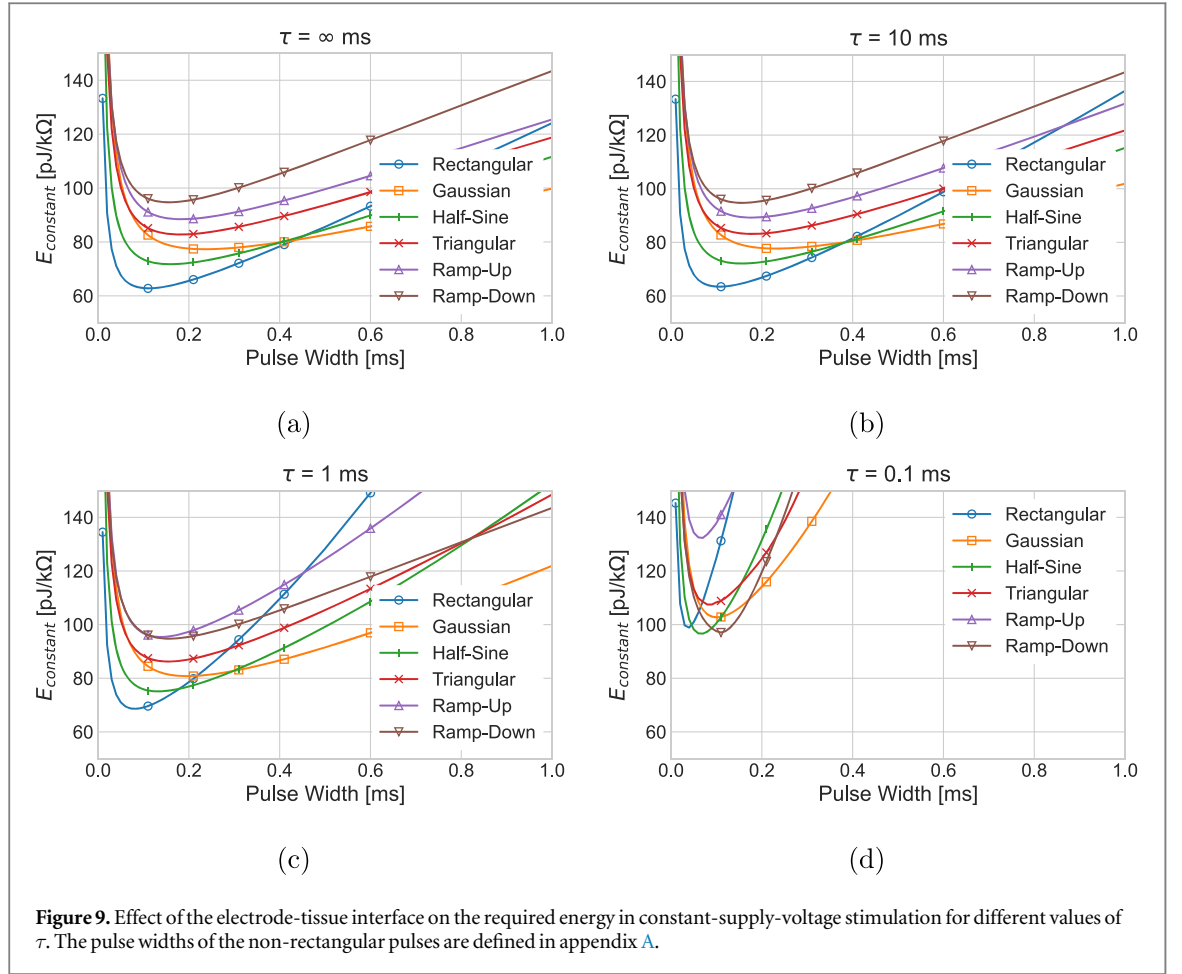
Figure 9. Effect of the electrode-tissue interface on the required energy in constant-supply-voltage stimulation for different values of τ. The pulse widths of the non-rectangular pulses are defined in appendix A.

Table 6. Current threshold ratio for which the required energy is equal to that of a rectangular pulse in case of a constant voltage supply.

Shape	Threshold ratio
Gaussian	$\approx \sqrt{6/\sqrt{2\pi}}$
Half-Sine	$\sqrt{\pi/2}$
Triangular	$\sqrt{2}$
Ramp-Up	$\sqrt{2}$
Ramp-Down	$\sqrt{2}$

that losses due to limited flexibility in the voltage supply negate potential energy reductions in the biological domain in the case of non-rectangular pulses. Previously, it was suggested that combining non-rectangular pulses with scaling of the supply to the minimum allowable voltage would result in the most energy-efficient way of stimulation [16]. The current results present an opposite finding that rectangular stimuli can be more energy efficient than the tested non-rectangular pulses in the case of a scalable, constant voltage supply. This provides a different perspective on pulse shaping and energy efficiency optimization of neural implants, specifically for large-scale multichannel systems where the flexibility of the voltage supply is limited.

Data availability statement

The data that support the findings of this study are available upon reasonable request from the authors.

Appendix A. Pulse shape definitions

The equations for the different pulse shapes are listed below. For all definitions, K_x is the peak amplitude, PW is the pulse width, and $u(t)$ is the unit step function. In the simulations of the Gaussian-shaped pulses, σ was set to PW/6.

Rectangular: $\quad I_{\text{stim}}(t) = K_r \cdot [u(t) - u(t - PW)]$

$$(1.1a)$$

$$\text{Ramp}-\text{up}: \quad I_{\text{stim}}(t) = K_{\text{ru}} \cdot \frac{t}{PW} \cdot [u(t) - u(t - PW)] \tag{1.1b}$$

$$\text{Ramp}-\text{down}: \quad I_{\text{stim}}(t) = K_{\text{rd}} \cdot \left(1 - \frac{t}{PW}\right) \cdot [u(t) - u(t - PW)] \tag{1.1c}$$

$$\text{Sine}: \quad I_{\text{stim}}(t) = K_{\text{s}} \cdot \sin\left(\frac{2\pi t}{2 \cdot PW}\right) \cdot [u(t) - u(t - PW)] \tag{1.1d}$$

$$\text{Gaussian}: \quad I_{\text{stim}}(t) = K_{\text{g}} \cdot \exp\left[-\frac{(t - PW/2)^2}{2\sigma^2}\right] \tag{1.1e}$$

$$\text{Triangular}: I_{\text{stim}}(t) = \begin{cases} K_{\text{t}} \cdot \frac{2t}{PW} & \text{for } 0 \leqslant t \leqslant \frac{PW}{2} \\ 2K_{\text{t}} - K_{\text{t}} \cdot \frac{2t}{PW} & \text{for } \frac{PW}{2} < t \leqslant PW \\ 0 & \text{otherwise} \end{cases} \tag{1.1f}$$

Appendix B. Axon fiber model parameters

Table B1. Model parameters for the single-axon fiber model.

Symbol	Description	Value
ρ_{a}	Axial resistivity	$100 \, \Omega \cdot \text{cm}$
σ_{o}	Extracellular conductivity	$0.276 \, \text{S} \cdot \text{m}^{-1}$
d_{m}	Diameter myelin sections	$1.25 \, \mu\text{m}$
d_{n}	Diameter nodal sections	$0.93 \, \mu\text{m}$
L_{n}	Length nodal sections	$1 \, \mu\text{m}$
L_{m}	Length myelin sections	$59 \, \mu\text{m}$
$C_{\text{m,n}}$	Membrane capacitance nodal sections	$1 \, \mu\text{F} \cdot \text{cm}^{-2}$
$C_{\text{m,m}}$	Membrane capacitance myelin sections	$0.02 \, \mu\text{F} \cdot \text{cm}^{-2}$
$R_{\text{m,n}}$	Membrane resistance nodal sections	$33.3 \, \text{k}\Omega \cdot \text{cm}^2$
$R_{\text{m,m}}$	Membrane resistance myelin sections	$1.125 \, \text{M}\Omega \cdot \text{cm}^2$
$\bar{g}_{\text{Nap}}$	Max. conductance persistent sodium	$6.83 \cdot 10^{-3} \, \text{S} \cdot \text{cm}^{-2}$
$\bar{g}_{\text{Nat}}$	Max. conductance transient sodium	$6.28 \, \text{S} \cdot \text{cm}^{-2}$
$\bar{g}_{\text{Kp}}$	Max. conductance persistent potassium	$9.74 \cdot 10^{-1} \, \text{S} \cdot \text{cm}^{-2}$
$\bar{g}_{\text{Kt}}$	Max. conductance transient potassium	$8.93 \cdot 10^{-2} \, \text{S} \cdot \text{cm}^{-2}$
$\bar{g}_{\text{Kv3.1}}$	Max. conductance A-type potassium	$5.18 \cdot 10^{-1} \, \text{S} \cdot \text{cm}^{-2}$
V_{Na}	Sodium reversal voltage	$50 \, \text{mV}$
V_{K}	Potassium reversal voltage	$-85 \, \text{mV}$
V_{L}	Leakage voltage	$-75 \, \text{mV}$
V_{rest}	Resting potential	$-80 \, \text{mV}$
T	Temperature	$37 \, °\text{C}$

ORCID iDs

Francesc Varkevisser ● https://orcid.org/0000-0003-4852-0550
Tiago L Costa ● https://orcid.org/0000-0002-0163-2435
Wouter A Serdijn ● https://orcid.org/0000-0003-4973-9677

References

[1] Fernández E, Alfaro A and González-López P 2020 Toward long-term communication with the brain in the blind by intracortical stimulation: challenges and future prospects *Frontiers in Neuroscience* **14** 681

[2] Shirafkan R and Shoaei O 2022 Current-Based Neurostimulation Circuit and System Techniques *Handbook of Biochips* (New York: Springer) pp 445–69

[3] van Dongen M N and Serdijn W A 2016 A power-efficient multichannel neural stimulator using high-frequency pulsed excitation from an unfiltered dynamic supply *IEEE Trans. Biomed. Circuits Syst.* **10** 61–71

[4] Foutz T J and McIntyre C C 2010 Evaluation of novel stimulus waveforms for deep brain stimulation *J. Neural Eng.* **7** 066008

[5] Wongsarnpigoon A and Grill W M 2010 Energy-efficient waveform shapes for neural stimulation revealed with a genetic algorithm *J. Neural Eng.* **7** 046009

[6] Eickhoff S and Jarvis J C 2020 An investigation of neural stimulation efficiency with gaussian waveforms *IEEE Trans. Neural Syst. Rehabil. Eng.* **28** 104–12

[7] Sahin M and Tie Y 2007 Non-rectangular waveforms for neural stimulation with practical electrodes *J. Neural Eng.* **4** 227–33

[8] Lee H M, Park H and Ghovanloo M 2013 A power-efficient wireless system with adaptive supply control for deep brain stimulation *IEEE J. Solid-State Circuits* **48** 2203–16

[9] Noorsal E, Sooksood K, Xu H, Hornig R, Becker J and Ortmanns M 2012 A Neural Stimulator Frontend With High-Voltage Compliance and Programmable Pulse Shape for Epiretinal Implants *IEEE J. Solid-State Circuits* **47** 244–56

[10] Arfin S K and Sarpeshkar R 2012 An energy-efficient, adiabatic electrode stimulator with inductive energy recycling and feedback current regulation *IEEE Trans. Biomed. Circuits Syst.* **6** 1–14

[11] Urso A, Giagka V, van Dongen M and Serdijn W A 2019 An ultra high-frequency 8-channel neurostimulator circuit With 68% peak power efficiency *IEEE Trans. Biomed. Circuits Syst.* **13** 882–92

[12] Rashidi A, Yazdani N and Sodagar A M 2021 Fully implantable, multi-channel microstimulator with tracking supply ribbon, multi-output charge pump and energy recovery *IET Circuits, Devices & Systems* **15** 104–20

[13] Williams I and Constandinou T G 2013 An energy-efficient, dynamic voltage scaling neural stimulator for a proprioceptive prosthesis *IEEE Trans. Biomed. Circuits Syst.* **7** 129–39

[14] Luo Z, Ker M-D, Yang T-Y and Cheng W-H 2017 A Digitally Dynamic Power Supply Technique for 16-Channel 12

V-Tolerant Stimulator Realized in a 0.18 μm 1.8-V/3.3-V Low-Voltage CMOS Process *IEEE Trans. Biomed. Circuits Syst.* **11** 1087–96

[15] Ha S, Akinin A, Park J, Kim C, Wang H, Maier C, Cauwenberghs G and Mercier P P 2015 A 16-channel wireless neural interfacing SoC with RF-powered energy-replenishing adiabatic stimulation *2015 Symposium on VLSI Circuits (VLSI Circuits). IEEE* pp C106–C107

[16] Foutz T J, Ackermann D M Jr., Kilgore K L and McIntyre C C 2012 Energy Efficient Neural Stimulation: Coupling Circuit Design and Membrane Biophysics *PLoS One* **7** e51901

[17] Aberra A S, Peterchev A V and Grill W M 2018 Biophysically realistic neuron models for simulation of cortical stimulation *J. Neural Eng.* **15** 066023

[18] Carnevale N T and Hines M L 2006 *The NEURON Book* (Cambridge: Cambridge University Press)

[19] Bossetti C A, Birdno M J and Grill W M 2008 Analysis of the quasi-static approximation for calculating potentials generated by neural stimulation *J. Neural Eng.* **5** 44–53

[20] Kolovou-Kouri K, Rashidi A, Varkevisser F, Serdijn W A and Giagka V 2022 Energy savings of multi-channel neurostimulators with non- rectangular current-mode stimuli using multiple supply rails *2022 44th Annual International Conference of the IEEE Engineering in Medicine & Biology Society (EMBC)*

[21] Merrill D R, Bikson M and Jefferys J G R 2005 Electrical stimulation of excitable tissue: design of efficacious and safe protocols *J. Neurosci. Methods* **141** 171–98

[22] Maynard E M, Nordhausen C T and Normann R A 1997 The utah intracortical electrode array: a recording structure for potential brain-computer interfaces *Electroencephalogr. Clin. Neurophysiol.* **102** 228–39

[23] Hasanuzzaman M, Motlagh B G, Mounaim F, Hassan A, Raut R and Sawan M 2018 Toward an energy-efficient high-voltage compliant visual intracortical multichannel stimulator *IEEE Trans. Very Large Scale Integr. VLSI Syst.* **26** 878–91

[24] Straka M M, Shafer B, Vasudevan S, Welle C and Rieth L 2018 Characterizing longitudinal changes in the impedance spectra of in-vivo peripheral nerve electrodes *Micromachines* **9** 587

[25] Monge M, Raj M, Nazari M H, Chang H-C, Zhao Y, Weiland J D, Humayun M S, Tai Y-C and Emami A 2013 A Fully Intraocular High-Density Self-Calibrating Epiretinal Prosthesis *IEEE Trans. Biomed. Circuits Syst.* **7** 747–60

[26] Lin C-Y, Li Y-J and Ker M-D 2012 High-voltage-tolerant stimulator with adaptive loading consideration for electronic epilepsy prosthetic SoC in a 0.18 μm CMOS process *10th IEEE International NEWCAS Conference. IEEE* pp 125–8

[27] Alonso F 2018 *Models and Simulations of the Electric Field in Deep Brain Stimulation : Comparison of Lead Designs, Operating Modes and Tissue Conductivity* Linköping University

[28] Reilly J and Diamant A M 2011 Waveform and Polarity Effects *Electrostimulation : Theory, Applications, and Computational Model* (Boston, United States: Artech House) pp 26–8

[29] Shepherd R K and Javel E 1999 Electrical stimulation of the auditory nerve: II. Effect of stimulus waveshape on single fibre response properties *Hear. Res.* **130** 171–88

[30] Grill W M 2015 Model-based analysis and design of waveforms for efficient neural stimulation *Progress in Brain Research* 222 (Amsterdam, The Netherlands: Elsevier) 147–62

[31] Ethier S and Sawan M 2011 Exponential current pulse generation for efficient very high-impedance multisite stimulation *IEEE Trans. Biomed. Circuits Syst.* **5** 30–8